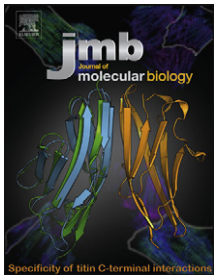

Structural Basis of Dynamic Membrane Recognition by trans-Golgi Network Specific FAPP Proteins

Marc Lenoir [1], Michał Grzybek [2,3], Michał Majkowski [4], Sandya Rajesh [1], Jaswant Kaur [1], Sara B.-M. Whittaker [1], Ünal Coskun [2,3] and Michael Overduin [1]

*1 - **School of Cancer Sciences,** College of Medical and Dental Sciences, University of Birmingham, Edgbaston, Birmingham B15 2TT, UK*
*2 - **Paul Langerhans Institute Dresden of the Helmholtz Centre Munich at the University Clinic and Medical Faculty Carl Gustav Carus,** TU Dresden, Fetscherstraße 74, 01307 Dresden, Germany*
*3 - **German Center for Diabetes Research (Deutsches Zentrum für Diabetesforschung e.V.),** Ingolstädter Landstraße 1, D-85764 Neuherberg, Germany*
*4 - **Laboratory of Cytobiochemistry,** Biotechnology Faculty, University of Wrocław, Przybyszewskiego 63-77, 51-148 Wrocław, Poland*

***Correspondence to Michael Overduin:** m.overduin@bham.ac.uk.*
http://dx.doi.org/10.1016/j.jmb.2014.12.023
Edited by M. Zhang

Abstract

Glycosphingolipid metabolism relies on selective recruitment of the pleckstrin homology (PH) domains of FAPP proteins to the trans-Golgi network. The mechanism involved is unclear but requires recognition of phosphatidylinositol-4-phosphate (PI4P) within the Golgi membrane. We investigated the molecular basis of FAPP1-PH domain interactions with PI4P bilayers in liposome sedimentation and membrane partitioning assays. Our data reveals a mechanism in which FAPP-PH proteins preferentially target PI4P-containing liquid disordered membranes, while liquid ordered membranes were disfavored. Additionally, NMR spectroscopy was used to identify the binding determinants responsible for recognizing trans-Golgi network-like bicelles including phosphoinositide and neighboring lipid molecules. Membrane penetration by the FAPP1-PH domain was mediated by an exposed, conserved hydrophobic wedge next to the PI4P recognition site and ringed by a network of complementary polar residues and basic charges. Our data illuminates how insertion of a structured loop provides selectivity for sensing membrane fluidity and targeting to defined membrane zones and organelles. The determinants of this membrane sensing process are conserved across the CERT, OSBP and FAPP family. Hence, lipid gradients not only result in differential membrane ordering along the secretory pathway but also specifically localize diverse proteins through recognition of ensembles of lipid ligands in dynamic and deformable bilayers in order to promote anterograde trafficking.

© 2015 Published by Elsevier Ltd.

Introduction

Diverse biological membranes within cells selectively recruit thousands of proteins using a phosphoinositide recognition code [1]. Such proteins transiently associate with membrane surfaces by recognizing phospholipids that exhibit organelle-specific distributions [2]. Cognate membrane complexes are further stabilized by complementary electrostatics [3–5] and insertion of nearby motifs of aliphatic, aromatic [6–8] or lipidated residues [9–11] into the bilayer. However, whether bilayer dynamics play a determining role in membrane recognition remains poorly defined [12,13], necessitating a closer examination of the structures of functional complexes.

The largest superfamily of membrane interactive proteins is that defined by the presence of pleckstrin homology (PH) domains. Its members include CERT, OSBP and FAPP (COF) proteins, which traffic ceramide, sterols and glycosphingolipids at the trans-Golgi network (TGN) [14–17]. Among them, the FAPP1 and FAPP2 proteins have become the best understood paradigms for recruitment to membranes enriched in phosphatidylinositol-4-phosphate (PI4P), which is the most abundant monophosphorylated inositol lipid in the Golgi membrane. Hence, their PH domains are often

used as Golgi markers in cellular studies [18,19]. However, the distribution of PI4P is not restricted to the Golgi apparatus, as this lipid signal also has critical roles beyond the Golgi [20]. Moreover, although COF family PH domains recognize PI4P physiologically [21–23], their *in vitro* PI specificities are not absolute [24–28]. This conundrum suggests that other conserved determinants also help to selectively attract these proteins to different organelle surfaces.

The two FAPP proteins differ mainly by the presence of a glycolipid transfer protein domain that is only found in the C-terminus of FAPP2 and that has a critical role in the intra-Golgi vectorial transfer of glucosylceramide [21,29] and in the synthesis of the globo series of glycosphingolipids [30]. Both their FAPP-PH domains possess a similar hydrophobic wedge that inserts into bilayers, although its contribution to ligand specificity remains unclear [27,28,31]. An analogous membrane insertion loop (MIL) is found in PI-binding FYVE and PX domains [32–34], with FAPP-PH domains being distinguished by Golgi-specific functions including membrane tubule budding and vesiculation [21,31].

Here, the structural basis of lipid-bilayer recognition by FAPP1 is resolved by analysis of protein partitioning into liposomal systems, mutagenesis and NMR. This yields experimental restraints for calculating the structure of ternary complexes of the protein with bound micelle and lipid ligand, thus explaining the requirement for loosely packed bilayers and pinpointing determinants for nonspecific and specific membrane engagement. We propose that modulation of PIs between microenvironments of varying membrane fluidity, as determined by the ratio of lipids including cholesterol and sphingomyelin (Fig. 1), provides a general switch for whether embedded lipid signals are accessible for protein recruitment at specific sub-organelle compartments.

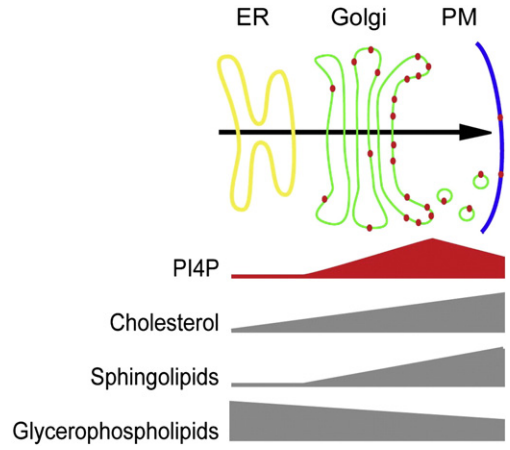

Fig. 1. The gradients of lipids are shown for the anterograde pathway from the endoplasmic reticulum (ER), where many are synthesized, through the Golgi where they and proteins are modified, to the plasma membrane (PM), and would influence the degree of lipid disorder in each compartment. The relative amount of PI4P within the compartments is illustrated by red dots.

Results

Specificity of FAPP-PH for disordered bilayers

In order to determine whether membrane order is important for FAPP-PH PI4P binding, we systematically explored sectors of the composition-dependent phase diagram of ternary lipid mixtures consisting of dioleoyl phosphatidylcholine (DOPC), cholesterol and brain sphingomyelin (BSM) [35–37] and supplemented them with 2% dipalmitoyl PI4P unless stated otherwise. Membrane order was validated with giant unilamellar vesicles (GUVs), employing fluorescent lifetime images with environmentally sensitive di-4-ANEPPDHQ (di-4) membrane reporter (Fig. S1). It was evident that association with PI4P-containing membranes decreased as ratios of both cholesterol and BSM increased. In pure liquid ordered (L_o) liposomes formed of an equimolar ratio of BSM and cholesterol, the FAPP1-PH domain interacted only marginally with the membrane (Fig. 2a).The most attractive PI4P-containing membranes were those forming liquid disordered (L_d) membrane phases (Fig. 2a), suggesting that lipid packing and dynamics could play a key role in efficient PI4P recognition and binding.

Next, we investigated the bilayer packing density as a function of the acyl chain saturation. The headgroups of dipalmitoyl phosphatidylcholine (DPPC), palmitoyl-oleyl phosphatidylcholine (POPC) and DOPC were compared as they occupy areas of 64, 68 and 72 nm^2, respectively, with concomitant effects on bilayer thickness [38]. Binding of FAPP1 to the set of PI4P/phosphatidylcholine (PC)-based liposomes revealed the highest level of binding to loosely packed DOPC vesicles: intermediate-density POPC vesicles exhibited medium binding, while the most densely packed DPPC vesicles excluded the FAPP1-PH (Fig. 2a). Thus, the lipid packing density was inversely related to protein binding. Hence, the membrane specificity of FAPP1-PH combines both essential chemical (i.e., PI4P) and physical (i.e., membrane fluidity) factors. Interestingly, this preference was also found with the full-length construct of FAPP2 (Fig. 2a), indicating broader relevance across the COF family.

The specific role played by membrane order in FAPP interactions with PI4P was further validated by fluorescent microscopy using GUVs. An equimolar ratio of cholesterol, DOPC and BSM was used to follow FAPP1-PH binding to PI4P in membranes exhibiting coexisting L_d and L_o domains. The fluorescent cholera toxin subunit (CTx) bound to the

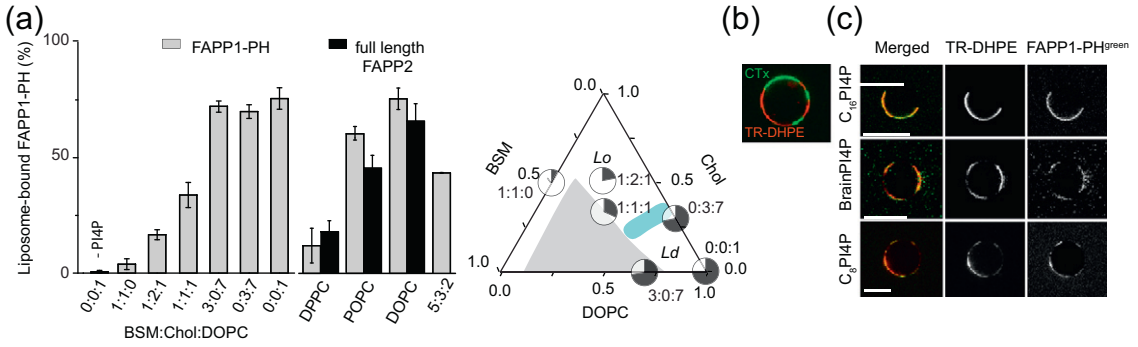

Fig. 2. FAPP-PH binds specifically to liquid disordered (L_d) phases. (a) Liposomes composed of BSM, cholesterol and DOPC ratios were selected from different regions of the ternary lipid phase diagram, as shown on the right, and the amount of bound protein was quantified by gel imaging. Unless stated otherwise, all liposomes contained 2% (mol/mol) PI4P. Data from liposomes composed of DPPC, POPC, DOPC or a mixture of DPPC, DOPC and cholesterol (5:3:2) is plotted on the left. The percentage of liposome-bound FAPP1-PH is indicated for each lipid composition. The phase diagram of DOPC, BSM and cholesterol mixtures is shown on the right. The regions of liquid ordered and disordered phases are indicated as L_o and L_d, respectively. These two phases coexist in vesicles formed by the lipid mixtures situated within the gray zone. The zone of transition between ordered and disordered vesicles is indicated in blue. (b) Disordered phases were monitored by the fluorescence signals of TR-DHPE and overlapped with FAPP1-PH^{green}. The bars in the confocal images represent 10 μm. (c) The PI4P ligand was included as either natural (brain extract) or synthetic (C_8 or C_{16}) forms in the vesicles formed by a 1:1:1 BSM:Chol:DOPC mixture and resulted in similar FAPP1-PH protein localization to the segregated disordered phase as revealed by the specific dyes TR-DHPE (L_d) and Oregon Green CTx (L_o) as seen by confocal microscopy.

ganglioside GM1 [39] and Texas Red-dihexadecanoyl phosphoethanolamine (TR-DHPE) [40] were used to mark the respective membrane domains, with the latter label preferentially partitioning to L_d domains (Fig. 2b). The presence of protein was detected by visualizing FAPP1-PH labeled with Oregon Green on an exposed unique cysteine (Cys37) (FAPP1-PH^{green}) (Fig. 2c). The FAPP1-PH^{green} protein localized strictly to L_d domains in phase-segregated GUVs, consistent with the liposome sedimentation experiments (Fig. 2a). Furthermore, this localization to disordered regions could be similarly mediated by either naturally (brain extract) or synthetically derived PI4P (dipalmitoyl or dioctanoyl) (Fig. 2c). This indicates that the phosphoinositide headgroup (rather than the respective acyl chains that differed) was the primary determinant of PI4P recognition in liquid disordered membrane regions. Binding to vesicles could be initiated by injecting soluble short-chain dioctanoyl (C_8) PI4P molecules into the chamber of reaction. In particular, an approximate 4-fold enhancement in protein colocalization with the disordered phase was observed after addition of 2 μM C_8-PI4P. This increase can be attributed in part to the inherent preference of short acyl chain lipids for disordered phases [41]. Thus, FAPP1-PH associates with L_d membrane phases potentially due to a favorable access to lipid headgroup, nonstereospecific contacts with PC molecules or suitable dynamics therein. Once bound to the disordered bilayer, the protein can conceivably diffuse laterally until it recognizes the headgroup of its PI4P ligand, thus forming a stable complex.

Bicelles mimic the bilayer for FAPP1-PH binding

Before characterizing the structural basis of dynamic bilayer recognition, we needed to select an appropriate bilayer mimic for quantitative analysis of the interactions. The binding of the FAPP1-PH domains with micelles and bicelles were compared as these both mimic biological bilayers and have different chain lengths and curvature properties. FAPP1-PH exhibited similar patterns of amide signal changes when bound to PI4P in the presence of micelles composed of *n*-dodecyl phosphocholine (DPC) or bicelles composed of dimyristoyl phosphatidylcholine (DMPC) and dihexanoyl phosphatidylcholine (DH_6PC), indicating consistent insertion modes. Moreover, their ligand affinities were similar, with the dispersed methyl resonance migrations yielding C_8-PI4P dissociation constants of 5.3 ± 2.4 μM and 8.8 ± 3.3 μM, (Fig. S2a and b), comparable to the affinity of small unilamellar vesicles (Fig. 6c). Furthermore, the chemical shifts of the protein bound to isotropic bicelles matched those of the state saturated with DPC:Chaps {3-[(3-cholamidopropyl)dimethylammonio]propanesulfonic acid} micelles. Minor spectral differences were observed between PI4P:micelle and PI4P:bicelle titrations. These arose largely from the absence of assigned cross-peaks from the bound states due to overlapped or broadened resonances. Thus, no significant difference was evident between micelle and bicelle complexes, and either state suitably represents how FAPP1-PH orients on bilayers *via* dynamic membrane insertion.

Resolving multistep bicelle binding by NMR

Previous studies have investigated how FAPP1-PH interacts with soluble PI4P molecules and associates with micelles [27], providing a basis for elucidating how the protein assembles on fluid bilayers that contain PI4P. In order to distinguish the determinants of transient nonspecific bilayer association and stable recognition of bilayer-embedded PI4P, we compared the binary and ternary complexes formed by FAPP1-PH, PI4P and micelles or bicelles in solution. This approach allowed identification of the multiple structural states formed by the FAPP1-PH domain as it interacts with membrane mimics of increasing size and complexity. First, the forms of FAPP1-PH saturated with micelle and bicelle were contrasted to identify the respective interactions and to model the PI4P-specific complexes formed. To gain maximal resolution, we characterized each state by monitoring backbone and side chain ^{1}H, ^{13}C and ^{15}N signals upon addition of soluble PI4P and stable bicelle formulations. Entry of the free state from solution into the bilayer was examined by tracking methyl and amide peaks as bicelles were added stepwise. This allowed the progressive changes induced by each binding event to be mapped at atomic resolution (Fig. 3a and b), showing that the interaction was principally mediated by the β1-β2 hairpin that spans FAPP1-PH residues Trp8 to Gln16, as was confirmed by results from paramagnetic relaxation enhancement (PRE) studies (Fig. 3c) [27]. Moreover, the data indicated a second, distal interaction site that includes the β6-β7 sheet residues Met61, Glu62, Leu63, Ile64, Glu68, His70 and Tyr72. Together, this provides experimental evidence for two-pronged stable insertion *via* the β1-β2 and β6-β7 elements.

Next, the structural orientation of the FAPP1-PH protein on bilayers was characterized by adding C_8-PI4P to the protein:micelle (Fig. 4a and d) and protein:bicelle assemblies (Fig. 4c and e). Intermolecular distance restraints were derived from doxylated lipid molecules (Figs. 3c and 4b) and soluble gadolinium agents (Fig. 5a and b). This illuminated the multiple states of free, nonspecifically PC associated and PI4P specifically bilayer bound protein, respectively. The experimental setup used to elucidate the structure of the micelle complex was adapted for bicelles, with the association being followed using PREs induced by paramagnetic gadolinium to identify solvent-exposed groups in the free, bicelle and bicelle-PI4P complexes. This general protocol provides a broadly applicable basis for experimentally based elucidation and validation of multiple bilayer-complexed structural states.

Structural basis of PI4P-bilayer recognition

Having defined the conditions for elucidating the consensus solution structure in bicelles and micelles, the wild-type FAPP1-PH domain responsible for dynamic bilayer insertion was determined by triple-resonance NMR methods. Its structure is largely identical with the mutant version solved previously (PDB ID 2KCJ), with chemical shift differences being localized to the wild-type Cys that had been previously replaced with a Ser to minimize opportunities for cross-linking. The structure of the monomeric native FAPP1-PH domain was defined by 1448

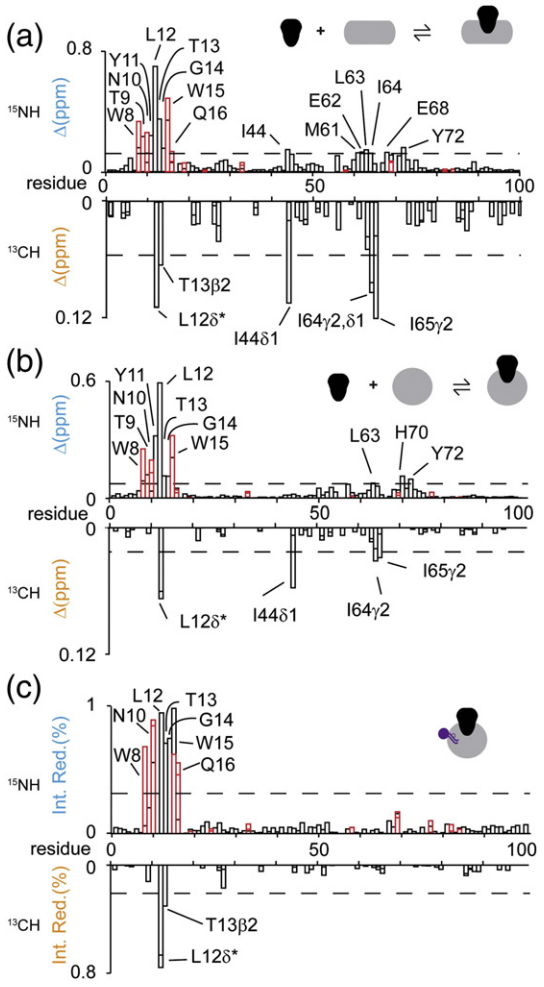

Fig. 3. NMR signal changes induced in FAPP1-PH by PI4P-independent bilayer binding. A transient interaction is evident from significant CSPs consistently induced by interactions with bicellar (a) and micellar (b) systems as measured from ^{15}N HSQC experiments in the absence of PI4P. This defined the active residues in HADDOCK calculations of the protein nonspecifically bound to the micelle. Backbone and side-chain resonance changes are indicated by black and red bars, respectively. (c) Distance restraints used to calculate the structural model were taken from PREs using doxyl-broadened FAPP1-PH resonances. Those restraints from ^{15}N and ^{13}C HSQC spectra are shown above and below the *x*-axes. Residues with significantly perturbed resonances (mean + standard deviation) are indicated. The inset cartoons show the relevant complex of protein, 5-doxyl PC and micelle in black, purple and gray, respectively, for each panel.

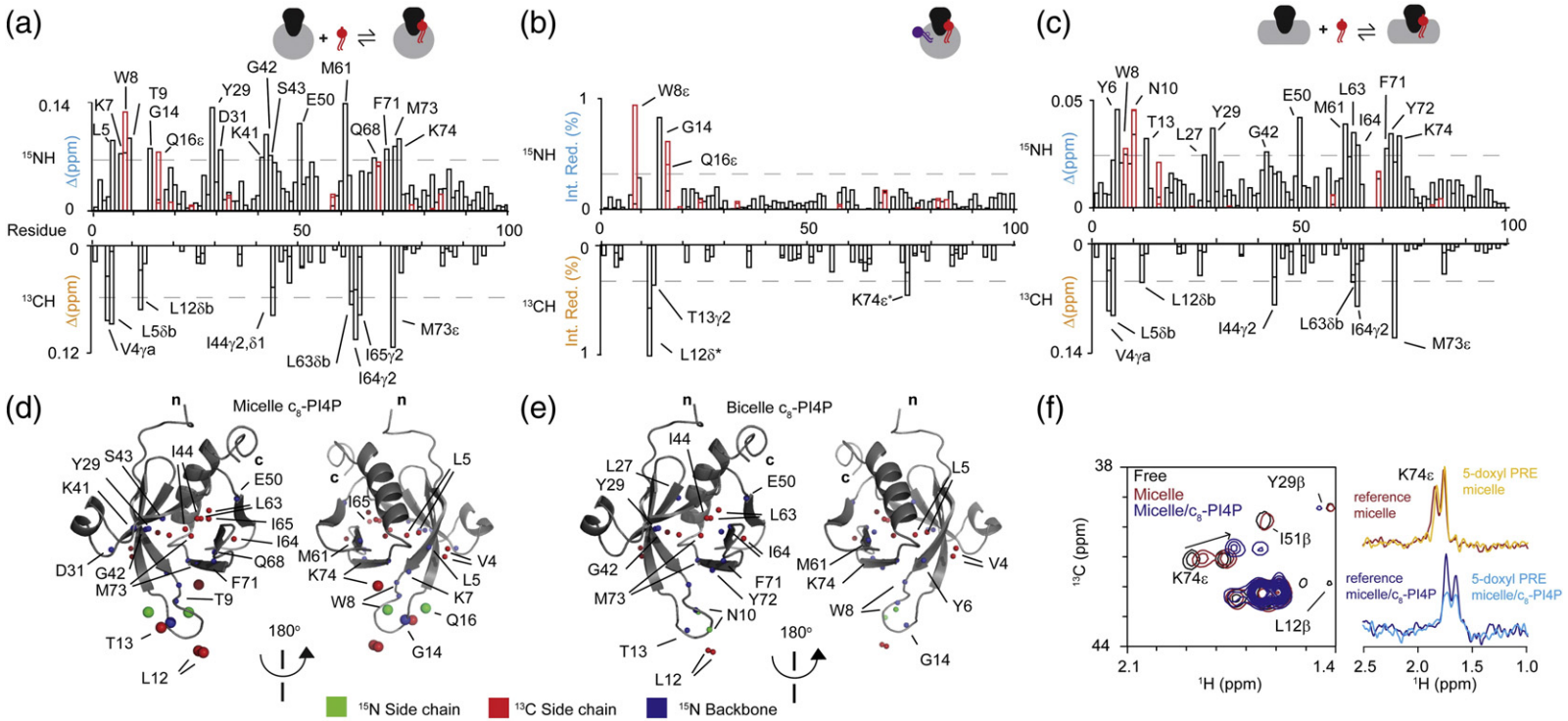

Fig. 4. Interaction of FAPP1-PH with PI4P assemblies. (a) The structural characterization of the specific complex was based on perturbations of FAPP1-PH resonances after addition of C_8-PI4P to samples containing $^{15}N/^{13}C$-labeled protein and either micelles or (c) bicelles. Chemical shift changes of ^{15}NH (top) and $^{13}CH_3$ (bottom) groups after addition of C_8-PI4P to samples containing 4 mM DPC:Chaps (3:1) micelles or 5% DH_6PC/DMPC bicelles are shown (b) as are PREs following addition of 5-doxyl PC-bound micelle *versus* PC:micelle controls, with the spin label shown as a red molecule in the cartoon. Black and red bars indicate backbone and side-chain signal perturbations, respectively. The dissociation constants of FAPP1-PH for C_8-PI4P-containing micelles and bicelles are 5.3 ± 2.4 μM and 8.8 ± 3.3 μM, respectively. Groups involved in micelle (d) and (e) bicelle binding based on CSPs and PREs upon PI4P addition are indicated as blue, green and red spheres in the structure for those groups with perturbed ^{15}N backbone, ^{15}N side-chain and ^{13}C methyl signals, respectively. Significant PREs are represented by large spheres. The ^{13}C HSQC spectra of FAPP1-PH from ligand titrations are superimposed with peaks of key residues labeled (f). The traces for the micelle-bound (red) and micelle/PI4P-bound state (blue) are shown in the left panel for Lys74ε side-chain resonance. Peak intensities for the diamagnetic and paramagnetic samples (red and yellow for micelle bound; blue and cyan for micelle/PI4P) are shown in the right panel.

distance-derived nuclear Overhauser enhancement (NOE), 128 dihedral angle and 34 hydrogen bond restraints, with the structural statistics being summarized in Table 1.

The micelle-complexed structure of the FAPP1-PH domain was solved using the HADDOCK program. The restraints included 16 intermolecular distances measured from ^{13}C methyl and ^{15}N amide-resolved PREs to the micelle, as obtained with the 5-doxyl PC spin label (Tables 1 and 2). A flexible zone of neighboring residues was defined as those that exhibited substantial chemical shift changes. Solvent accessibility data was derived from titrating in the gadolinium agent into ^{15}N and ^{13}C isotopically labeled protein samples. Bicelles composed of diheptanoyl phosphatidylcholine (DH7PC) and DMPC (q = 0.3, 0.25%) were added stepwise. The advantage of the new bicelle formulation over conventional bicelles composed of DH_6PC and DMPC formulations was apparent as small increments could be added from initial concentrations as low as 0.1% (w/v). This enabled monitoring of the bicelle-bound state during titration experiments. This formulation was optimized for low concentrations [43] and adapted herein to track protein resonances while conserving a signal that was sufficiently strong and resolved to be useful for PRE analysis. The solvent-exposed and micelle-embedded protein surfaces were mapped by analysis of PRE data collected using water-soluble gadolinium or doxyl PC spin labels, respectively, thus defining their complementary areas (Fig. 5a–c). Interfacial residues were defined as being those with resonances that were broadened by both gadolinium and doxylated phospholipid. Together, this provided cross-validated definition of the FAPP1-PH protein groups that were exposed, interfacial or deeply inserted.

The structural model of the complex based on PRE data reveals that membrane recruitment of FAPP1 involved deep insertion of Tyr11 and Leu12. Their side chains penetrated furthest into the hydrophobic interior of the bilayer, while they formed a solvent-exposed extremity at the tip of the structured β1-β2 loop in solution. Their side chains orient beneath the surface of phospholipid headgroups in either the micelle or the bicelle complex in the presence or absence of PI4P, indicating a constitutive role in insertion. Moreover, the specific PI4P recognition event uniquely involved insertion of the side chain of β7 residue Lys74. This

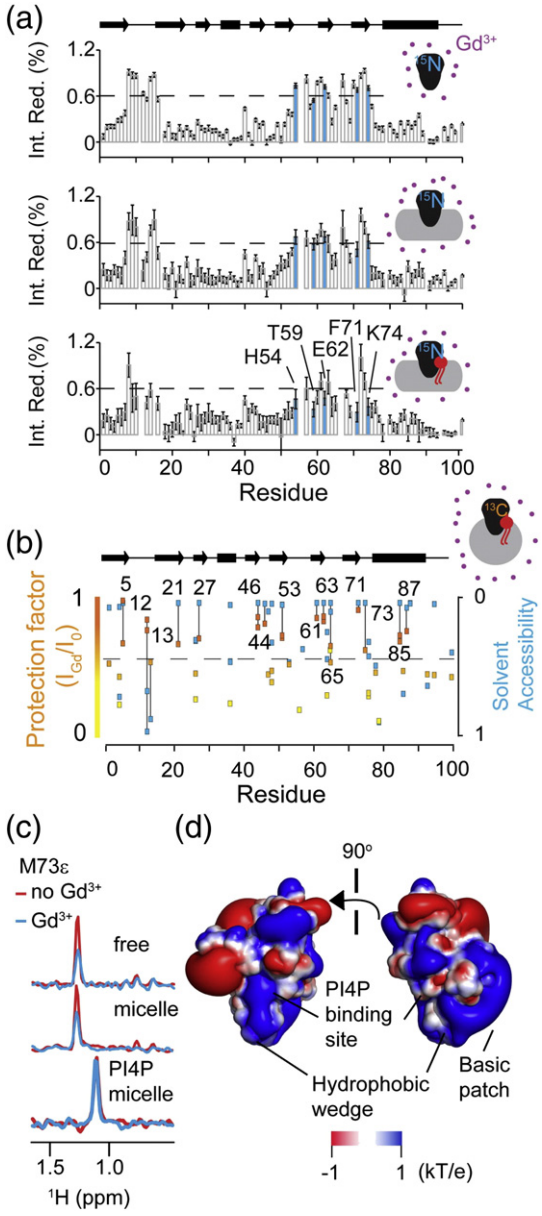

Fig. 5. The solvent-exposed surface of bilayer-bound FAPP1-PH mapped by PREs. (a) The gadodiamide (Gd^{3+})-induced PREs are expressed as a percentage of reduction of the signal intensity observed in paramagnetic *versus* diamagnetic samples. The intensity reduction of backbone amide signals of each residue of the free state of FAPP1-PH (top) and the bicelle-bound (middle) and bicelle:PI4P-complexed (bottom) forms are shown. The residues indicated in the lower panel and colored blue exhibit a significant change in solvent accessibility upon formation of the bicelle:PI4P:FAPP1-PH complex. (b) The protection factors for ^{13}C methyl groups of FAPP1-PH bound to PI4P-containing micelle are plotted. The color gradient indicates the degree of solvent protection. The *y*-axis corresponds to the solvent accessibility calculated with NACCESS for the free state of FAPP1-PH. Protected methyl groups are indicated with vertical lines. (c) The one-dimensional traces were extracted from two-dimensional ^{13}C HSQC spectra (red, diamagnetic; blue, paramagnetic) showing the Met73Cε resonance of the free state, FAPP1-PH:micelle and FAPP1-PH:micelle:PI4P complexes. (d) Electrostatic maps of the FAPP1-PH structure calculated with APBS [42] showing the isocontours and superimposed with the surface accessible area (between −1 and 1 kT/e). FAPP1-PH is oriented as in Fig. 4d.

Table 1. NMR and refinement statistics for solution structures and micelle-docked structures.

Solution structure of FAPP1-PH		
NMR distance and dihedral constraints		
Distance constraints		
Total NOE	1448	
Unambiguous	1223	
Long range ($\|i-j\|>5$)	235	
Medium ($4\le\|i-j\|\le5$)	41	
Short ($2\le\|i-j\|\le3$)	83	
Sequential/intra	864	
Ambiguous	225	
Hydrogen bonds	34	
Total dihedral angle restraints	128	
φ, ψ	64, 64	
Structure statistics		
Violations		
Distance constraints (Å) (>0.5 Å)	0	
Dihedral angle constraints (°)	0	
Deviations from idealized geometry		
Bond lengths (Å)	0.006573 ± 0.000167	
Bond angles (°)	0.791 ± 0.016	
Impropers (°)	1.777 ± 0.089	
Average pairwise RMSD[a] (Å)		
Heavy, backbone	0.86, 0.32	
Energies (kcal/mol)		
E_{noe}	442.77 ± 10.85	
E_{cdih}	6.25 ± 1.63	
E_{bond}	74.39 ± 3.73	
$E_{improper}$	109.62 ± 8.94	
E_{angle}	295.85 ± 12.06	
E_{vdw}	−185.74 ± 26.89	
E_{dihe}	582.8 ± 7.53	
Ramachandran statistics[b]		
Residues in core regions (%)	73.86	
Residues in allowed regions (%)	22.33	
Residues in generous regions (%)	2.5	
Residues in disallowed regions (%)	1.4	
Docked structures	**Micelle**	**Micelle:PI4P**
Intermolecular energies		
Buried surface (Å^2)	1208.22 ± 125.87	1232.09 ± 117.94
E_{vdw} (kcal/mol)	−58.50 ± 5.26	−59.29 ± 6.05
E_{elec} (kcal/mol)	−80.48 ± 39.22	−122.72 ± 33.94
Insertion		
θ (°)	16.80 ± 4.50	14.23 ± 4.32
ψ (°)	166.52 ± 16.29	153.52 ± 30.39
r (mass centers) (Å)	38.47 ± 1.00	37.14 ± 1.13
Interactions[c]	8, **10**, **11**, 12, 13, 15, **16**	**8**, **10**, **11**, 12, **13**, **15**, **16**, **74**

[a] RMSD is calculated for secondary structural elements including residues 1–7, 16–22, 26–30, 43–44, 50–53, 61–64, 69–73 and 78–94 calculated for ten representative structures.
[b] Non-glycine residues.
[c] More than 7 of the 20 models. Boldfaced residues are hydrogen bonded between the headgroups of DPC and W8ε, N10δ, T13, W15ε, Q16ε and K74ε.

basic residue is conserved across the COF protein family members and interfaces peripherally with the bilayer (Fig. 4f), thus contributing to the higher affinity of the PI4P-containing membrane complex.

The deep burial of the Leu12 and Thr13 methyl groups was confirmed by the substantial changes in solvent accessibility observed after gadolinium addition (Fig. 5b). These residues were encircled by an extensive network of interfacial contacts mediated by polar backbone and side-chain groups of residues in the β1-β2 loop including Asn10 and Gln16, which form hydrogen bonds and ionic interactions with PC headgroups (Table 1). The Trp8 and Trp15 residues act as aromatic buttresses against the membrane surface (Fig. 6a and b), delimiting the total buried surface area of either 1208 Å^2 or 1232 Å^2 between the protein and the micelle in the absence or presence of PI4P, respectively. This insertion element is ordered with the exception of the most exposed Leu12 residue based on model-free relaxation analysis (Fig. S3) [45].

Table 2. Experimental data used for deriving structural restraints to model the FAPP1-PH interaction with PI4P membrane mimicking micelles in the HADDOCK calculations based on an established approach [44].

Lipid model	NMR data	Nuclei	Resonance
Micelle (PI4P+DPC)	5-doxyl PC PRE	^{15}N	Trp8ε, Gly14, Q16ε Asn10, Asn10δ, Leu12, Thr13, Trp15, Trp15ε
		^{13}C	Leu12δ, Thr13γ, Lys74ε
	CSP	^{15}N	Leu5, Lys7-Gln16, Ile 44, Ile 63-Ile65, Glu68, His70, Phe72, Met73, Trp8ε
		^{13}C	Val4γ, Leu5δ, Leu12δ, Ile 44, Ile63δ-Ile65γ, Met73ε
Bicelles	Gd^{3+} spin label	^{15}N	Thr9, Asn10 ,Thr13, Gly14, Ser53, Thr59,Glu62, Ile71,Lys74
		^{13}C	Leu12δ, Thr13γ
	CSP	^{15}N	Tyr6, Trp8, Trp8ε, Asn10, Asn10δ, Thr13, Lys27, Tyr29, Gly42, Glu50, Met61, Leu63, Ile64, Ile64, Ile71, Tyr72, Lys74
		^{13}C	Leu12δ, Thr13γ, Ile63β, Ile64γ
Loss of function by mutation			
K7A, W8E, W8Y, N10T, Y11G, L12G, Q16R, R18L			
HADDOCK restraints			
Deeply inserted	Trp8ε, Asn10(N,δ), Leu12(N,δ), Thr13(N,γ), Gly14N, Trp15(N,ε), Gln16ε		
Interfacial	Lys74ε		

Together, this reveals that overlapping structured protein surfaces mediate transient nonspecific and PI4P-specific binding of fluid-bilayer phases, respectively. Thus, we infer that initial, weak bilayer entry of the β1-β2 loop with primarily loosely packed PC molecules leads to a PI4P-dependent adjustment of the orientation of the inserted complex.

The structural organization with the ternary FAPP1-PH:PI4P:bilayer complex can be ascertained by NMR following C_8–PI4P addition to the micelle complex. Phosphoinositide addition results in the unprecedented stable micelle burial of the Met73 side chain in the β7 strand. Considering the absence of 5-doxyl PRE effects in the Met73 resonances, this change in exposure could be due to its enclosure within the stable PI4P:micelle complex (Fig. 5c). This indicates a PI4P ligand-dependent bilayer interaction by this structured element, with the proximal Leu63 and Ile64 residues also engaged based on their chemical shift changes. This ternary complex exhibits a slower off-rate and extensive zone of perturbations midway between the most deeply inserted β1-β2 extremity and the exposed termini (Fig. 4d and e). The large perturbed zone observed in the PI4P-specific complex involves all the β strands including β1: Val4-Tyr6, β2:Thr13, β3:Leu27,Tyr29, β4:Gly42, β5: Glu50, β6:Met6,Leu63,Ile64 and β7:Phe71-Lys74 residues (Fig. 4d and e). The micelle-based burial of these residues was confirmed by changes in solvent accessibility upon addition of the paramagnetic gadodiamide agent, with a broader interface being buried when PI4P was present, including His54, Thr59, Glu62, Phe71 and Lys74 (Fig. 5a). Together, with the entire lower half of the protein exhibiting chemical shift perturbations (CSPs) and the interfacial position of the β5-β7 sheet, this indicates that specific recognition of PI4P-containing bilayers involves stable rather than transient dipping of the hydrophobic β1-β2 tip into the bilayer interior [27] and adjustment to a more substantially buried state.

In addition to the hydrophobic contribution, it is well known that electrostatics also influence the orientation

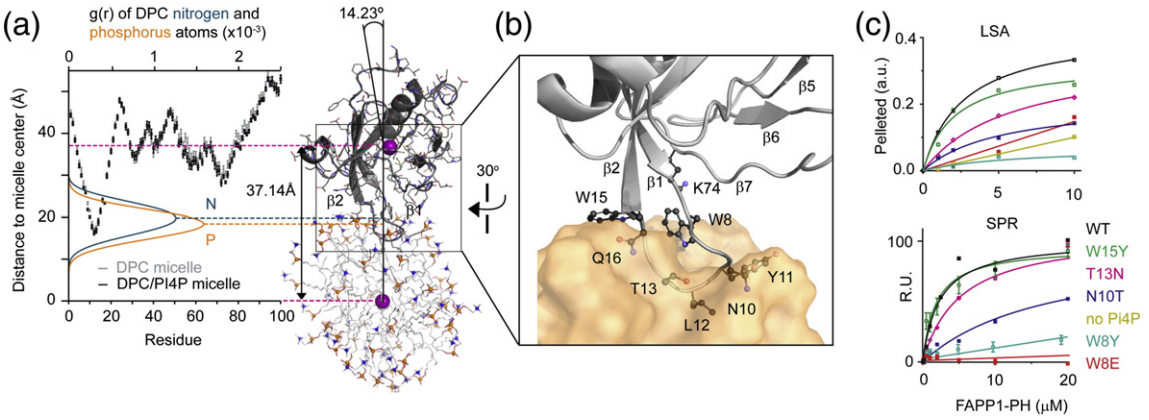

Fig. 6. FAPP1-PH membrane binding. (a) Comparison of pure and PI4P-containing micelle-docked structural orientations. Back-calculated distances (micelle center to protein backbone HNs) for the 20 best models of micelle-bound (gray) and PI4P-bound (black) models are represented. Micelle and protein centers are indicated by purple dotted lines, the radial distribution [$g(r)$] of phosphorus (yellow) and nitrogen (blue) atoms of the choline headgroups is indicated by small spheres. The radial distributions were calculated from a 200-ps free molecular dynamic calculations in explicit water within Xplor. The structure closest to the mean is shown with the distance between the protein and micelle centers labeled, as well as the change in insertion angle upon PI4P binding by the micelle complex. The β1 and β2 strands are indicated. (b) A detailed model of FAPP1-PH showing the side chains (balls and sticks) is shown. The micelle surface (orange) and β strands are indicated as are the key interfacial residues. The hydrophobic wedge is delimited by Trp8 and Gln16 and is oriented such that β2 is fully inserted into micelles while β1 is interfacial. Residues with significant PREs are shown. (c) Mutations of membrane inserting residues reduce affinities for PI4P-containing membranes based on liposome sedimentation assays and SPR. The cosedimented fraction and relative response units are plotted for different FAPP1-PH concentrations.

of proteins on membrane surfaces. Indeed, this is reflected by the dipolar nature of the FAPP1-PH surface (Fig. 5d). Two distinct positively charged isocontours facing the micellar interface correspond to the PI4P binding pocket and elements of the β7 strand including the Lys74 side chain [23]. The resulting electrostatic complementarily could account for the 2-fold increase in binding affinity observed when negatively charged phosphatidylserine is added to the membrane to stabilize the specific PI4P-containing complex [27]. Indeed, analogous preferences for phosphatidylserine co-association is apparent in PI3P-specific FYVE and PX domains [46,47], indicating a wider role for this accessory phospholipid as a codeterminant of intracellular membrane binding.

Table 3. Dissociation constants measured for FAPP1-PH membrane interactions.

Protein	Dissociation constant estimated from	
	Liposome sedimentation assays (μM)	SPR (μM)
WT	2.05 ± 0.90	2.68 ± 0.71
W8E	>1000	>1000
W8Y	>1000	>1000
N10T	5.12 ± 1.07	17.32 ± 5.74
T13F	5.1	n.d.[a]
T13N	5.86 ± 0.83	5.15 ± 0.54
W15Y	2.67 ± 0.09	2.48 ± 0.61
W15E	n.d.[a]	n.d.[a]
Q16R	>1000	>1000
R18L	>1000	>1000

[a] Not determined due to the instability of the mutant.

The ring of charge encircling FAPP1's hydrophobic MIL appears to delimit the depth of membrane insertion. In order to estimate the depth and angle of protein penetration into the bilayer in nonspecific and specific membrane engagement, we compared how FAPP1-PH inserted into PI4P-free *versus* PI4P-containing micelles, taking advantage of the sensitivity of the NMR method to even transient interactions. The methyl and amide PRE data yielded average distances of 38.47 Å and 37.14 Å between protein and micelle centers, indicating similar depths in the specific and nonspecific membrane complexes, respectively (Figs. 3, 4 and 6a). That is, the specific complex penetrated only an angstrom deeper and its insertion angle was only slightly more acute. This can be attributed to PI4P-containing micelle contacts formed by Lys74, the neighboring β5-β6 and β6-β7 loops and the extremity of the β1-β2 hairpin. PI4P binding by the micelle-saturated complex also induced alterations in hydrophobic core packing of the protein based on perturbations of methyl resonances of either partially buried Val4 and Ile64 residues or completely buried Leu5, Ile44, Leu63, Ile65 and Met73 residues. We propose that this network reinforces the slowly exchanging PI4P-bilayer complex and increases the residency time and local concentration of protein molecules on membranes. Upon bilayer association, the hydrophobic wedge of the FAPP1-PH domain is not symmetrically inserted. Rather, it is oriented such that

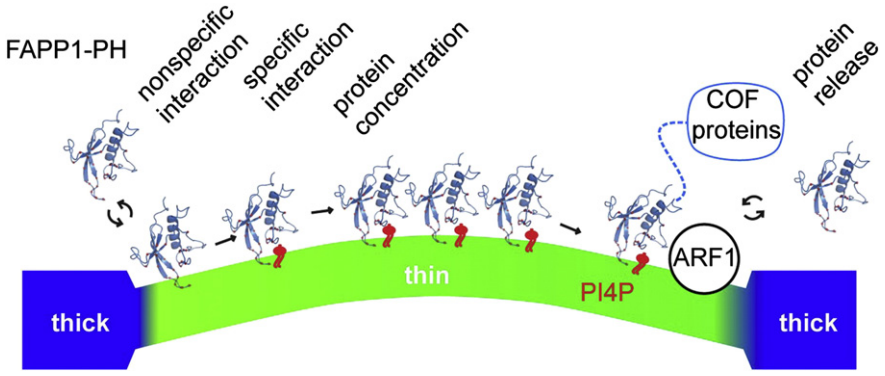

Fig. 7. Membrane binding model. The proposed states of FAPP proteins at the TGN involve nonspecific insertion into the loosely packed bilayer regions (green), diffusing laterally until a PI4P molecule (red) is encountered and bound, thus increasing the residency time such that protein accumulates and boosting lateral pressure in the bilayer. The proposed membrane recognition by the PH domain and Arf1 interaction could be extended to other COF family proteins to drive specific organelle targeting. Lipids transferred by COF proteins to the membrane increase the membrane rigidity and result in a progressive release of the PH domain of the COF proteins, thus halting the activity of COF proteins.

the backbone residues prior to the β2 strand (Thr13, Gly14 and Trp15) deeply insert into micelles while the backbone of conserved residues following the β1 strand binds the interfacial inositide headgroup *via* Trp8 and Thr9 contacts. The local ring of basic charge capped by an acidic patch (Fig. 5d) provides long-range guidance for the protein's entry into the membrane. Together, this allows progressive binding and tilting of the bilayer complex and could have implications for interaction of downstream protein partners such as Arf1 with TGN vesiculation machinery [48].

Mutational analysis of membrane binding determinants

The residues identified in the structural model as membrane interacting were mutated to delineate their roles. All mutants were tested for being structurally intact and functionally altered (Table S1). Binding of FAPP-PH proteins to membranes was measured using liposome sedimentation experiments. The most deeply inserted Tyr11 and Leu12 side chains are known to be essential [31], but the contributions of other residues of the loop, including Trp8, Asn10, Thr13, Trp15 and Gln16 residues, have not been determined. Each Trp residue extends its side chain to pack against the micelle surface and hence was mutated to an Ala, a Glu or a Tyr residue. The W8E and W8Y mutants of FAPP1-PH did not bind detectably (Table 3 and Fig. 6c), indicating that Trp8 makes critical contributions in both nonspecific and specific membrane complexes. This is consistent with its interfacial positions in the binary and ternary structures with PI4P and micelle.

Mutations of the nonconserved Thr13 residue were designed to conserve the hydrogen bond acceptor (T13N) and to alter the exposed hydrophobicity (T13F). Both mutations were tolerated with only minor reductions in binding by a factor of 2, consistent with the peripheral role of Thr13 in nonspecific insertion. Moreover, Thr13 is not conserved across the COF family, which maintains basic or small hydrophilic residues at this position [27]. Conversely, the N10T mutation compromised bilayer affinity by a small but significant degree, as can be explained by the insertion of its side chain between PC-based headgroups and its role in hydrogen bonding (Table 2). The substitution of Trp15 with a Tyr (but not Glu, which results in unstable protein) was tolerated, consistent with the critical role of its aromatic ring in insertion and stabilizing the β1-β2 hairpin. The replacement of Gln16 with an Arg residue was originally intended to mimic the polybasic motif found in PH domains that recognizes 3-phosphoinositides [49]. Unexpectedly, this mutation reduced liposome association, independent of the phosphoinositide species used. The major role of Gln16, which is strictly conserved across the mammalian COF family, can be explained by the hydrogen bonds it consistently forms with PC molecules when fully docked.

Together, this reveals that liquid disordered membrane interaction is mediated by essentially the entire breadth of the ordered β1-β2 hairpin loop (Fig. S3), which is ordered except for the hydrophobic tip. In particular, the hydrophobic extremity offered by Tyr11 and Leu12 is bordered by nonessential Asn10 and Thr13 contacts, and the highly conserved aromatic groups contributed by Trp8 and Trp15 form critical struts against disordered bilayer surfaces. We propose that sliding of this structured loop through the leaflet allows the protein to diffuse in the two dimensional plane of a membrane, with electrostatic forces supporting the protein's positioning on the bilayer for PI headgroup entry. Once a PI4P molecule is bound, the mobility of the resulting complex would be reduced by the additional bound bulk, and the conformational dynamics in the

protein-bilayer complex including in angle and depth of insertion and core packing would shift to that of the fully occupied state. The accompanying displacement of lipid molecules and resulting perturbation of local pressure and surface area created could contribute to the deformation of membranes during budding or tubulation events.

Discussion

The ability of FAPP proteins to specifically recognize PI4P-enriched Golgi membranes is determined by a set of unique features that are revealed here by NMR. The mechanism involves proximal penetration of the structured MIL residues and PI4P acyl chains into a liquid disordered bilayer, introducing substantial protein volume into the leaflet. This insertion would naturally yield positive local curvature and hence would be opposed by the tendency of cholesterol to induce negative membrane curvature. The FAPP1-PH domain inserts deeply *via* not only the longest structured MIL studied to date but also by the β7 strand, as supported in the case of FAPP1 by ^{13}C- and ^{15}N-resolved backbone and side-chain groups for micelle- or bicelle-embedded and soluble spin labels. The use of both heteronuclei for gathering PRE restraints and the use of optimized bicelles yielded the highest density of experimental protein-bilayer structural restraints to date to our knowledge.

TGN-bilayer binding mediated by FAPP1-PH is initiated by nonspecific phospholipid interaction followed by specific binding to a PI4P molecule. These events differ surprisingly little in the depth or angle of bilayer penetration. The most significant differences are the structuring of the PI4P site and conformational adjustment within the core as the ligand is bound. This yields a slowly exchanging complex with a binding affinity of 5 μM for the monomeric protein. The fact that the MIL is largely structured is unanticipated given its long and irregular nature, as is the β7 binding element, yet could explain their specificity for dynamic bilayers. The interfacial region involves functionally critical tryptophans of the loop and cationic residues that engage the surface of the bilayer and support the orientation of the embedded protein. In particular, Trp8 and Trp15 form struts at either extremity of the MIL, while Lys74 is opposite the PI4P binding site and forms hydrogen bonds with the membrane surface. These aromatic and basic residues are highly conserved in the FAPP family and occupy similar positions around the basic patch of the CERT structure [23], inferring a common mechanism.

This general FAPP-bilayer binding mechanism is depicted in Fig. 7. The process involves the electrostatic approach and insertion of the FAPP1 protein into disordered bilayer within a restricted membrane territory [50]. The resulting reorientation of lipids within the leaflet includes displacement of dynamic lipid allowing PI4P molecules to be more readily encountered before being stably bound within the appropriately positioned PI4P site. The resulting asymmetric insertion of protein bulk within the bilayer would induce local positive bilayer curvature. Interestingly, the insertion depth and angle are only slightly perturbed by the transition from nonspecific to specific complex; instead, the original contacts become reinforced, resulting in the tighter FAPP:PI4P complex becoming specifically localized and crowded within dynamic TGN zones. This process leaves a complementary site on the FAPP1-PH domain largely available for Arf1 docking [48] that is necessary but not sufficient to localize FAPPs at the TGN [21]. We note that, while preparing this manuscript, a study addressed the mechanism of yeast Arf1 binding to human FAPP1-PH [51] and is largely consistent with our results.

The crucial role of the various COF proteins in lipid trafficking [16,29,30,52] suggests that they share recognition determinants. The commonalities are most obvious for CERT [17,53] and OSBP1 [54], localization of which has also been linked to Golgi membrane composition. The key residues are shared across the COF family, inferring similar assembly and membrane deformation processes. In phase-segregated GUVs, the preference seen for L_d domains is such that these proteins could all be essentially completely directed only to disordered phases (Fig. 7). *In vitro*, such proteins would become crowded until reaching a critical concentration where buds form and tubules can then emanate. Biological membrane tubule formation by FAPPs has yet to be confirmed under physiological conditions. Nonetheless, tubules have been observed *in vitro* [31] and in cell-based assays [18,21], and specific roles of contributing residues can now be tested in cellular TGN systems. Broader applicability of the general mechanism to other systems can be envisaged. Lipid enzymes may be similarly regulated by bilayer order. For example, PI4P kinase type IIα, which produces half of the PI4P at the Golgi, is active once bound there within rigid microdomains [55].

In summary, we propose that membrane malleability represents a fundamental means of controlling protein recruitment to specific regions of organelles such as Golgi subcompartments. In endomembranes, lipid concentration gradients across the secretory pathway are found in opposing directions (Fig. 1), with the ratio of glycerophospholipids decreasing and sphingolipids and cholesterol increasing [56,57]. Moreover, the saturation of the acyl chains for different lipid species increases along the anterograde pathway [58]. As a result, both the membrane rigidity and thickness are enhanced as one travels from the endoplasmic reticulum toward the plasma membrane, with the TGN having an intermediate lipid composition prone

to phase separations [59]. Hence, a membrane-order-dependent PI4P binding model would account for the absence of FAPPs at the plasma membrane despite pools of PI4P having been identified there [18]. Furthermore, changes of membrane rigidity could efficiently control the recruitment of COF proteins to the TGN to maintain local lipid homeostasis. Thus, as sphingolipids and cholesterol are recruited at the TGN by leaving vesicles, reduced membrane packing densities would lead to an enhanced lipid transfer rate of FAPP2 (glucosylceramide), CERT (ceramide) and OSBP (sterol) that would progressively re-establish the rigidity, acting as a negative feedback loop on the lipid transfer proteins. In other words, PI4P molecules in membranes with opposing membrane fluidities could simplistically represent "on" and "off" signaling states for recruiting FAPP proteins to regions in the TGN membrane gradients. Although PI4P is present in other subcellular membranes where it critically contributes to other biological processes [20], it may not be visible there to these proteins due to its ordered microenvironment. An analogous phenomenon has been invoked for recognition of the sphingolipid GM1 by cholera toxin B subunit [60,61]. The presence of cholesterol in the membranes forced GM1 headgroups to bend, into a conformational state where the toxin no longer recognizes them. Thus, we propose that this principle of binary lipid order recognition states also applies to other phosphoinositides and lipids, which may be similarly visible or invisible to binding partners depending on the local conformational dynamics of the membrane [62].

Materials and Methods

Protein expression

FAPP1-PH was expressed in a pGEX-6P-1 vector (GE Healthcare, Little Chalfont, UK) as a glutathione *S*-transferase (GST) fusion protein and purified as previously described [27]. Uniform isotopic labeling with ^{15}N or $^{13}C/^{15}N$ was carried out in M9 media. The cell lysate was passed through a GST Trap column and the protein was cleaved overnight using Prescission protease (GE Healthcare). The FAPP1-PH protein was separated by anion exchange using a linear gradient of NaCl from 0 to 0.5 M [20 mM Tris (pH 8)] and was exchanged into 20 mM Tris (pH 7), 100 mM NaCl, 1 mM DTT and 1 mM NaN_3 (TB). The mutants were generated with a QuikChange lightening kit (Stratagene, Santa Clara, USA) and verified by DNA sequencing. The proteins were expressed and purified as previously described [27] using optimized salt gradients to separate FAPP and GST proteins during the final purification step.

Protein fluorescent tagging

Conjugation of FAPP1-PH protein to the Oregon Green maleimide fluorescent probe (Life Technologies, Carlsbad, USA) was performed according to the manufacturer's protocols. Briefly, complete reduction of disulfide bonds was achieved in TB with 10 mM DTT for 1 h. Subsequently, the sample of 100 μM protein was buffer exchanged with TB and incubated for 4 h at room temperature with maleimide fluorescent probe in a 10× excess and purified on PD-10 columns.

Lipid binding assays

Lipids, detergents and natural extract of PI4P (brain extract) were purchased from Avanti Polar Lipids (Alabaster, USA) and synthetic phosphoinositides including C_8-PI4P were from Echelon Biosciences (Salt Lake City, USA). Micelle and bicelle titration experiments were carried out by stepwise additions of buffer-matched stock solutions into NMR samples. Bicelles were generated using DMPC and DH_6PC mixed in chloroform, dried under a flux of nitrogen and left under high vacuum overnight. A stock solution at 25% was prepared and diluted with the protein immediately before each experiment. Bicelles with a ratio $q = 0.25$ were used at a 5% (w/v) to prevent excessive line broadening and alignment of the bicelles with the magnetic field. Bicelles containing diheptanoyl phosphatidylcholine and DMPC ($q = 0.3$, 0.25%) were prepared for acquisition of ^{15}N-edited heteronuclear single quantum coherence (HSQC) experiments.

Lipids were mixed in chloroform, the organic solvent was successively dried under a nitrogen stream and samples were placed under high vacuum overnight. The lipids were resuspended in TB to a lipid concentration of 2 mM, and suspension was submitted to 10 cycles of freezing in liquid N_2 and thawing at 52 °C. For the assays, 75 μL of the lipid suspension was mixed with 25 μL of protein at 8 μM and incubated at room temperature for 10 min. The pellet collected after centrifugation (55,000 rpm, 4 °C, 10 min) with a TLA-55 rotor (Beckman Coulter, High Wycombe, UK) was washed three times with TB and resuspended in 100 μL. The supernatant and the pellet of each assay were loaded on precast 26-well Criterion gel (Biorad, Hemel Hempstead, UK). After electrophoresis, the proteins were stained by Coomassie blue and quantified by gel imaging (Syngene, Cambridge, UK). Values represent the mean and standard deviations from triplicate experiments.

Surface plasmon resonance

The surface plasmon resonance (SPR) experiments were carried out in TB on a Biacore 3000 instrument using sensor Chip L1 (GE Healthcare). A suspension of 1 g/L lipids DOPC:PI4P (98:2) or DOPC was submitted to 10 FAT cycles and extruded through a 100-nm membrane (Avestin). A total of 150 μL of this lipid suspensions were coated on the lanes at 5 μL/min, washed with 10 mM NaOH and coated with 25 μL bovine serum albumin and were cleaned again with 10 mM NaOH. Equilibrium measurements were carried out at 2–3 μL/min, and the sensograms were obtained for an analyte range 0.1–20 μM and corrected by subtracting the reference signals from the DOPC lanes. The apparent dissociation constant was deduced from the fitting $B = B_{max} \cdot P_{free}/(K_d + P_{free})$

where B is the binding, B_{max} is the maximum signal under saturation and P_{free} is the concentration of protein present in the solution injected. In all experiments, the response of FAPP1-PH^{WT} at 20 μM was chosen as standard to normalize the response of the mutants.

GUV formation

A volume of 25 μL of the lipid mixtures at 1 g/L in chloroform was spread on ITO-coated slides (Sigma) and dried under vacuum for at least 2 h. GUVs were grown at 52 °C in 150 mM sucrose. A sinusoidal current (1.1 Vpp, 12 Hz) was applied for 2–3 h followed by a squared current (1.5 Vpp, 5 Hz). The GUVs were collected and resuspended in a Tris buffer [10 mM (pH 7); 50 mM NaCl and 1 mM DTT]. Chambers were built using double-sided tapes and the passivation of the surface was achieved with a solution containing 1 mg/mL of casein. After washing with resuspending buffer, we injected the GUVs into the observation cell. Alternatively, glass bottom dishes (MatTek, Ashland, USA) were used for microscopic observations to allow uniform injections across the sample. To visualize different phases, we included GM1 at 1% (mol/mol) in the lipid mixtures. The fluorescent probes cholera toxin subunit B tagged with AlexaFluor 488 (CTx) (Life Technologies) and Texas Red 1,2-dihexadecanoyl-*sn*-glycero-3-phosphoethanolamine (TR-DHPE) (Life Technologies) were used to mark ordered and disordered phases, respectively. The image processing and were performed within ImageJ software [63]. Green-emitting dyes were excited at 488 nm and red-emitting dyes were excited at 543 nm.

Fluorescence lifetime imaging microscopy

GUVs were prepared according to established methods [64] and stained with 2 μM di-4-ANEPPDHQ (di-4) dye (Invitrogen). Fluorescence lifetime imaging microscopy was performed at 23 °C with an LSM 510 microscope (Carl Zeiss) equipped with a dedicated PicoQuant fluorescence lifetime imaging microscopy system. The probe was excited with a 473-nm pulsed laser diode (50 MHz) and observed with a 63× oil immersion objective and fluorescence was collected through a 495-nm, long-wave pass filter. Laser power was adjusted to give an average photon rate of 10^4–10^5 photons to avoid pile-up effects. The acquisition time was of the order of 200 s to achieve at least 10^3 photons per pixel.

Thermal shift assay

In order to determine the stabilities of mutant proteins, we measured fluorescent signals using excitation at 492 nm and emission at 568 nm from solutions containing 4 μM protein and SYPRO Orange (Life Technologies) in 50 mM Hepes buffer (pH 7) and 100 mM NaCl. Signals were followed along a linear temperature gradient between 25 °C and 95 °C. The experiments were carried out on an MxPro3005P qPCR detection system and processed with MxPro software (Stratagene). The unfolding transition temperature, T_m, of each protein corresponded to the point of inflexion of the curves [65].

Nuclear magnetic resonance spectroscopy

NMR experiments were acquired at 298 K on an 800-MHz Varian INOVA spectrometer or a 600-MHz Bruker AVANCE III spectrometer equipped with 5-mm cryogenic probes, using samples containing 100–700 μM FAPP1-PH protein. Slowly exchanging amide protons were identified from ^{15}N HSQC spectra acquired following dissolution in 99.96% D_2O. Backbone and side-chain resonances were assigned in part by referring to those of the C94S mutant protein. NMR experiments were run using Varian BioPack pulse sequences, including BEST HNCO, HNCA, HN(CO)CA and ^{13}C-edited NOESY-HSQC (100 ms mixing time), acquired from ^{13}C/^{15}N-labeled protein samples containing 10% D_2O. The ^{15}N relaxation experiments were acquired using pulse sequences available in the Bruker standard library and with ^{15}N-labeled protein.

Backbone generalized order parameters squared, S^2, were determined with the model-free formalism [66,67] from ^{15}N relaxation data using the diffusion tensor obtained for an axially symmetric motional model. The ^{15}N R_1 and R_2 relaxation rates and {^{1}H}-^{15}N heteronuclear NOE values for FAPP1-PH were measured at a ^{1}H frequency of 600 MHz at 298 K using established methods [68,69]. To estimate the R_1 and R_2 values, we fit monoexponential two-parameter decay functions to peak intensity *versus* measured relaxation delay profiles using the Analysis program from the CcpNmr software suite [70]. NOE values were determined from the ratio of peak intensity in the proton-saturated spectrum *versus* peak intensity in the unsaturated spectrum for a given resonance. Errors were calculated from repeat measurements (R_1 and R_2) or from an analysis of background noise in the spectrum when repeat spectra were not available. For model-free analysis, an initial estimate of the rotational diffusion tensor was obtained from the R_2/R_1 ratios of individual so-called "rigid" residues and the PDB coordinates of the FAPP1-PH solution structure using the programs pdbinertia, r2r1_diffusion and quadric_diffusion (A. G. Palmer, Columbia). Residues were considered rigid if they satisfied the following criteria: (1) NOE > 0.65 and (2) of the remaining residues, $\langle R_2 \rangle - R_{2,n} < 1$ SD (where SD is standard deviation from the mean $\langle R_2 \rangle$). Fitting of the R_2/R_1 ratios from 51 rigid residues in total was performed using different rotational diffusion tensors: isotropic, axial and fully anisotropic with established model selection criteria [71]. Amide proton-nitrogen bond lengths of 1.02 Å and ^{15}N chemical shift anisotropy of −160 ppm were assumed for all residues. Order parameters were subsequently determined following the flowchart of Mandel *et al.*, using their software ModelFree v. 4.2 [71] and FAST ModelFree [72]. Uncertainties in the model-free order parameters were estimated from 500 Monte Carlo simulations.

PRE experiments were performed as described elsewhere [27]. DPPC was substituted for 5-doxyl PC in reference experiments to ensure that only 5-doxyl-dependent NMR intensity differences were measured. The gadodiamide agent (Selleckchem, Newmarket, UK) was added to protein:lipid assemblies in NMR samples from a concentrated stock solution in NMR buffer. The chemical shifts perturbations were calculated as $\Delta = (\Delta^2_{HN} + \alpha\Delta^2_{HX})^{1/2}$ where α is the ratio of the magnetic ratios of nuclei (0.1 for X = ^{15}N and 0.25 for X = ^{13}C). The dissociation constant K_d was calculated from $\Delta = \Delta_{max}(L_T + P_T + K_d - [(L_T + P_T + K_d)^2 - 4L_TP_T]^{1/2})/2P_T$ where L_T and P_T are the ligand and protein concentrations

and Δ represents the chemical shift change. The CSPs were calculated with 2 mM DPC:Chaps as a reference to account for possible nonspecific interactions of unimolecular PC molecules in solution. The perturbations were calculated relative to micellar concentrations while bicelle-dependent changes were measured in reference to a protein NMR sample free of any lipid. The NMR spectra were processed using NMRPipe [73], and the resonance assignments and the structure calculations were carried out in CcpNmr analysis suite and Aria2 [74], respectively. The structures were generated by restrained torsion angle dynamics in eight iterations using Aria2. After a final water refinement, the 20 lowest-energy structures out of 100 calculated were selected to represent the ensemble of FAPP1-PH structures (see details in Supplementary Information). The coordinates and resonance assignment were deposited at the PDB and Biological Magnetic Resonance Bank [75] databases under the identifiers 2MDX and 19508, respectively.

Molecular docking

Flexible docking of FAPP1-PH and micelle structures was carried out using an established protocol [44]. Developments incorporated here include the detection of buried $^{1}H,^{13}C$-group PREs from doxyl PC and solvent-exposed groups from the gadolinium agent. Briefly, the active residues were defined based on chemical shift changes induced by micelle and bicelle, and the solvent accessibility was estimated with NACCESS. Ambiguous distance restraints between the micelle center and protein groups were set for atoms significantly broadened by 5-doxyl micelles. The docking protocol began with 400 randomly oriented and spatially separated protein and micelle structures taken from the representative ensembles.

Database linking

The structure of wild-type human FAPP1-PH domain sequence is linked in PDB ID 2MDX and the corresponding Biological Magnetic Resonance Bank entry 19508.

Acknowledgements

We thank Christian Ludwig for help with NMR spectra acquisition and discussions; Arthur Palmer for software for dynamics analysis; Elena Odintsova for assistance with confocal microscopy; the Wellcome Trust, HWB-NMR and Bio-NMR for supporting facility access; and the Biotechnology and Biological Sciences Research Council, Cancer Research UK and the European Union PRISM project for funding (M.O.). M.G. and U.C were supported by funds of the Deutsche Forschungsgemeinschaft (Transregio 83) and by the German Federal Ministry of Education and Research (Bundesministerium für Bildung und Forschung) Grant in support of the German Center for Diabetes Research (Deutsches Zentrum für Diabetesforschung e.V.)

Appendix A. Supplementary data

Supplementary data to this article can be found online at http://dx.doi.org/10.1016/j.jmb.2014.12.023.

Received 17 September 2014;
Received in revised form 17 December 2014;
Accepted 29 December 2014
Available online 8 January 2015

Keywords:
pleckstrin homology domain;
lipid microdomains;
membrane trafficking;
phosphoinositide recognition;
nuclear magnetic resonance spectroscopy

Abbreviations used:
BSM, brain sphingomyelin; COF, CERT, OSBP and FAPP; DH PC, dihexanoyl phosphatidylcholine; DMPC, dimyristoyl phosphatidylcholine; DOPC, dioleoyl phosphatidylcholine; $_{6}$ GST, glutathione *S*-transferase; GUV, giant unilamellar vesicle; MIL, membrane insertion loop; NOE, nuclear Overhauser enhancement; PC, phosphatidylcholine; POPC, palmitoyl-oleyl phosphatidylcholine; PH, pleckstrin homology; PI4P, phosphatidylinositol-4-phosphate; SPR, surface plasmon resonance; TGN, trans-Golgi network; TR-DHPE, Texas Red-dihexadecanoyl phosphoethanolamine.

References

[1] Overduin M, Cheever ML, Kutateladze TG. Signaling with phosphoinositides: better than binary. Mol Interv 2001;1:150–9.
[2] Roth MG. Phosphoinositides in constitutive membrane traffic. Physiol Rev 2004;84:699–730.
[3] Heyningen SV. Cholera toxin: interaction of subunits with ganglioside GM1. Science 1974;183:656–7.
[4] Klee CB. Ca^{2+}-dependent phospholipid- (and membrane-) binding proteins. Biochemistry 1988;27:6645–53.
[5] Ellson CD, Gobert-Gosse S, Anderson KE, Davidson K, Erdjument-Bromage H, Tempst P, et al. PtdIns(3)P regulates the neutrophil oxidase complex by binding to the PX domain of p40(phox). Nat Cell Biol 2001;3:679–82.
[6] Peter BJ, Kent HM, Mills IG, Vallis Y, Butler PJ, Evans PR, et al. Embo JBAR domains as sensors of membrane curvature: the amphiphysin BAR structure. Science 2004;303:495–9.
[7] Frost A, Perera R, Roux A, Spasov K, Destaing O, Egelman EH, et al. Structural basis of membrane invagination by F-BAR domains. Cell 2008;132:807–17.
[8] Mim C, Cui H, Gawronski-Salerno JA, Frost A, Lyman E, Voth GA, et al. Structural basis of membrane bending by the N-BAR protein endophilin. Cell 2012;149:137–45.
[9] Aicart-Ramos C, Valero RA, Rodriguez-Crespo I. Protein palmitoylation and subcellular trafficking. Biochim Biophys Acta 1808;2011:2981–94.
[10] Franco M, Chardin P, Chabre M, Paris S. Myristoylation-facilitated binding of the G protein ARF1GDP to membrane phospholipids is required for its activation by a soluble nucleotide exchange factor. J Biol Chem 1996;271:1573–8.

[11] Navarro-Lerida I, Sanchez-Perales S, Calvo M, Rentero C, Zheng Y, Enrich C, et al. A palmitoylation switch mechanism regulates Rac1 function and membrane organization. EMBO J 2012;31:534–51.
[12] Rocks O, Peyker A, Kahms M, Verveer PJ, Koerner C, Lumbierres M, et al. An acylation cycle regulates localization and activity of palmitoylated Ras isoforms. Science 2005; 307:1746–52.
[13] Safouane M, Berland L, Callan-Jones A, Sorre B, Romer W, Johannes L, et al. Lipid cosorting mediated by shiga toxin induced tubulation. Traffic 2010;11:1519–29.
[14] Lagace TA, Byers DM, Cook HW, Ridgway ND. Altered regulation of cholesterol and cholesteryl ester synthesis in Chinese-hamster ovary cells overexpressing the oxysterol-binding protein is dependent on the pleckstrin homology domain. Biochem J 1997;326:205–13.
[15] Hanada K, Kumagai K, Yasuda S, Miura Y, Kawano M, Fukasawa M, et al. Molecular machinery for non-vesicular trafficking of ceramide. Nature 2003;426:803–9.
[16] D'Angelo G, Polishchuk E, Di Tullio G, Santoro M, Di Campli A, Godi A, et al. Glycosphingolipid synthesis requires FAPP2 transfer of glucosylceramide. Nature 2007;449:62–7.
[17] Tuuf J, Kjellberg MA, Molotkovsky JG, Hanada K, Mattjus P. The intermembrane ceramide transport catalyzed by CERT is sensitive to the lipid environment. Biochim Biophys Acta 1808;2011:229–35.
[18] Balla A, Tuymetova G, Tsiomenko A, Varnai P, Balla T. A plasma membrane pool of phosphatidylinositol 4-phosphate is generated by phosphatidylinositol 4-kinase type-III alpha: studies with the PH domains of the oxysterol binding protein and FAPP1. Mol Biol Cell 2005;16:1282–95.
[19] Vermeer JEM, Thole JM, Goedhart J, Nielsen E, Munnik T, Gadella TWJ. Imaging phosphatidylinositol 4-phosphate dynamics in living plant cells. Plant J 2009;57:356–72.
[20] Hammond GR, Machner MP, Balla T. A novel probe for phosphatidylinositol 4-phosphate reveals multiple pools beyond the Golgi. J Cell Biol 2014;205:113–26.
[21] Godi A, Di Campli A, Konstantakopoulos A, Di Tullio G, Alessi DR, Kular GS, et al. FAPPs control Golgi-to-cell-surface membrane traffic by binding to ARF and PtdIns(4)P. Nat Cell Biol 2004;6:393–404.
[22] Levine TP, Munro S. The pleckstrin homology domain of oxysterol-binding protein recognises a determinant specific to Golgi membranes. Curr Biol 1998;8:729–39.
[23] Sugiki T, Takeuchi K, Yamaji T, Takano T, Tokunaga Y, Kumagai K, et al. Structural basis for the Golgi-association by the pleckstrin homology domain of the ceramide trafficking protein CERT. J Biol Chem 2012;287:33706–78.
[24] Kam JL, Miura K, Jackson TR, Gruschus J, Roller P, Stauffer S, et al. Phosphoinositide-dependent activation of the ADP-ribosylation factor GTPase-activating protein ASAP1. Evidence for the pleckstrin homology domain functioning as an allosteric site. J Biol Chem 2000;275:9653–63.
[25] Shinozaki-Narikawa N, Kodama T, Shibasaki Y. Cooperation of phosphoinositides and BAR domain proteins in endosomal tubulation. Traffic 2006;7:1539–50.
[26] Kavran JM, Klein DE, Lee A, Falasca M, Isakoff SJ, Skolnik EY, et al. Specificity and promiscuity in phosphoinositide binding by pleckstrin homology domains. J Biol Chem 1998; 273:30497–508.
[27] Lenoir M, Coskun U, Grzybek M, Cao X, Buschhorn SB, James J, et al. Structural basis of wedging the Golgi membrane by FAPP pleckstrin homology domains. EMBO Rep 2010;11:279–84.
[28] Levine TP, Munro S. Targeting of Golgi-specific pleckstrin homology domains involves both PtdIns 4-kinase-dependent and -independent components. Curr Biol 2002;12:695–704.
[29] Vieira OV, Gaus K, Verkade P, Fullekrug J, Vaz WL, Simons K. FAPP2, cilium formation, and compartmentalization of the apical membrane in polarized Madin-Darby canine kidney (MDCK) cells. Proc Natl Acad Sci USA 2006;103: 18556–61.
[30] D'Angelo G, Uemura T, Chuang CC, Polishchuk E, Santoro M, Ohvo-Rekila H, et al. Vesicular and non-vesicular transport feed distinct glycosylation pathways in the Golgi. Nature 2013;501:116–20.
[31] Cao X, Coskun U, Rossle M, Buschhorn SB, Grzybek M, Dafforn TR, et al. Golgi protein FAPP2 tubulates membranes. Proc Natl Acad Sci USA 2009;106:21121–5.
[32] Kutateladze T, Overduin M. Structural mechanism of endosome docking by the FYVE domain. Science 2001;291:1793–6.
[33] Cheever ML, Sato TK, de Beer T, Kutateladze TG, Emr SD, Overduin M. Phox domain interaction with PtdIns(3)P targets the Vam7 t-SNARE to vacuole membranes. Nat Cell Biol 2001;3:613–8.
[34] Xing Y, Liu D, Zhang R, Joachimiak A, Songyang Z, Xu W. Structural basis of membrane targeting by the Phox homology domain of cytokine-independent survival kinase (CISK-PX). J Biol Chem 2004;279:30662–9.
[35] Veatch SL, Keller SL. Separation of liquid phases in giant vesicles of ternary mixtures of phospholipids and cholesterol. Biophys J 2003;85:3074–83.
[36] Roux A, Cuvelier D, Nassoy P, Prost J, Bassereau P, Goud B. Role of curvature and phase transition in lipid sorting and fission of membrane tubules. EMBO J 2005;24:1537–45.
[37] Veatch SL, Keller SL. Seeing spots: complex phase behavior in simple membranes. Biochim Biophys Acta 2005;1746: 172–85.
[38] Lindblom G, Oradd G. Lipid lateral diffusion and membrane heterogeneity. Biochim Biophys Acta 2009;1788:234–44.
[39] Dietrich C, Volovyk ZN, Levi M, Thompson NL, Jacobson K. Partitioning of Thy-1, GM1, and cross-linked phospholipid analogs into lipid rafts reconstituted in supported model membrane monolayers. Proc Natl Acad Sci USA 2001;98: 10642–7.
[40] Baumgart T, Hunt G, Farkas ER, Webb WW, Feigenson GW. Fluorescence probe partitioning between Lo/Ld phases in lipid membranes. Biochim Biophys Acta 2007;1768: 2182–94.
[41] Mesquita RM, Melo E, Thompson TE, Vaz WL. Partitioning of amphiphiles between coexisting ordered and disordered phases in two-phase lipid bilayer membranes. Biophys J 2000;78:3019–25.
[42] Baker NA, Sept D, Joseph S, Holst MJ, McCammon JA. Electrostatics of nanosystems: application to microtubules and the ribosome. Proc Natl Acad Sci USA 2001;98:10037–41.
[43] Lu Z, Van Horn WD, Chen J, Mathew S, Zent R, Sanders CR. Bicelles at low concentrations. Mol Pharm 2012;9:752–61.
[44] Dancea F, Kami K, Overduin M. Lipid interaction networks of peripheral membrane proteins revealed by data-driven micelle docking. Biophys J 2008;94:515–24.
[45] Berjanskii MV, Wishart DS. A simple method to predict protein flexibility using secondary chemical shifts. J Am Chem Soc 2005;127:14970–1.
[46] Kutateladze TG, Capelluto DG, Ferguson CG, Cheever ML, Kutateladze AG, Prestwich GD, et al. Multivalent mechanism of membrane insertion by the FYVE domain. J Biol Chem 2004;279:3050–7.

[47] Lee SA, Kovacs J, Stahelin RV, Cheever ML, Overduin M, Setty TG, et al. Molecular mechanism of membrane docking by the Vam7p PX domain. J Biol Chem 2006;281:37091–101.
[48] He J, Scott JL, Heroux A, Roy S, Lenoir M, Overduin M, et al. Molecular basis of phosphatidylinositol 4-phosphate and ARF1 GTPase recognition by the FAPP1 pleckstrin homology (PH) domain. J Biol Chem 2011;286:18650–7.
[49] Ferguson KM, Kavran JM, Sankaran VG, Fournier E, Isakoff SJ, Skolnik EY, et al. Structural basis for discrimination of 3-phosphoinositides by pleckstrin homology domains. Mol Cell 2000;6:373–84.
[50] Bigay J, Antonny B. Curvature, lipid packing, and electrostatics of membrane organelles: defining cellular territories in determining specificity. Dev Cell 2012;23:886–95.
[51] Liu Y, Kahn RA, Prestegard JH. Interaction of Fapp1 with Arf1 and PI4P at a Membrane Surface: An Example of Coincidence Detection. Structure 2014;22:421–30.
[52] Halter D, Neumann S, van Dijk SM, Wolthoorn J, de Maziere AM, Vieira OV, et al. Pre- and post-Golgi translocation of glucosylceramide in glycosphingolipid synthesis. J Cell Biol 2007;179:101–15.
[53] Perry RJ, Ridgway ND. Oxysterol-binding protein and vesicle-associated membrane protein-associated protein are required for sterol-dependent activation of the ceramide transport protein. Mol Biol Cell 2006;17:2604–16.
[54] Nhek S, Ngo M, Yang X, Ng MM, Field SJ, Asara JM, et al. Regulation of oxysterol-binding protein Golgi localization through protein kinase D-mediated phosphorylation. Mol Biol Cell 2010;21:2327–37.
[55] Lu D, Sun HQ, Wang H, Barylko B, Fukata Y, Fukata M, et al. Phosphatidylinositol 4-kinase IIalpha is palmitoylated by Golgi-localized palmitoyltransferases in cholesterol-dependent manner. J Biol Chem 2012;287:21856–65.
[56] Holthuis JC, Pomorski T, Raggers RJ, Sprong H, Van Meer G. The organizing potential of sphingolipids in intracellular membrane transport. Physiol Rev 2001;81:1689–723.
[57] van Meer G, Voelker DR, Feigenson GW. Membrane lipids: where they are and how they behave. Nat Rev Mol Cell Biol 2008;9:112–24.
[58] Schneiter R, Brugger B, Sandhoff R, Zellnig G, Leber A, Lampl M, et al. Electrospray ionization tandem mass spectrometry (ESI-MS/MS) analysis of the lipid molecular species composition of yeast subcellular membranes reveals acyl chain-based sorting/remodeling of distinct molecular species en route to the plasma membrane. J Cell Biol 1999;146:741–54.
[59] Klemm RW, Ejsing CS, Surma MA, Kaiser HJ, Gerl MJ, Sampaio JL, et al. Segregation of sphingolipids and sterols during formation of secretory vesicles at the trans-Golgi network. J Cell Biol 2009;185:601–12.
[60] Lingwood D, Simons K. Lipid rafts as a membrane-organizing principle. Science 2010;327:46–50.
[61] Sezgin E, Chwastek G, Aydogan G, Levental I, Simons K, Schwille P. Photoconversion of bodipy-labeled lipid analogues. Chembiochem 2013;14:695–8.
[62] Czogalla A, Grzybek M, Jones W, Coskun Ü. Validity and applicability of membrane model systems for studying interactions of peripheral membrane proteins with lipids. Biochim Biophys Acta Mol Cell Biol Lipids 2014;1841:1049–59.
[63] Schneider CA, Rasband WS, Eliceiri KW. NIH Image to ImageJ: 25 years of image analysis. Nat Methods 2012;9:671–5.
[64] Bagatolli LA, Gratton E. A correlation between lipid domain shape and binary phospholipid mixture composition in free standing bilayers: A two-photon fluorescence microscopy study. Biophys J 2000;79:434–47.
[65] Ericsson UB, Hallberg BM, Detitta GT, Dekker N, Nordlund P. Thermofluor-based high-throughput stability optimization of proteins for structural studies. Anal Biochem 2006;357:289–98.
[66] Lipari G, Szabo A. Model-free approach to the interpretation of nuclear magnetic resonance relaxation in macromolecules. 2. Analysis of experimental results. J Am Chem Soc 1982;104:4559–70.
[67] Lipari G, Szabo A. Model-free approach to the interpretation of nuclear magnetic resonance relaxation in macromolecules. 1. Theory and range of validity. J Am Chem Soc 1982;104:4546–59.
[68] Farrow NA, Muhandiram R, Singer AU, Pascal SM, Kay CM, Gish G, et al. Backbone dynamics of a free and phosphopeptide-complexed Src homology 2 domain studied by ^{15}N NMR relaxation. Biochemistry 1994;33:5984–6003.
[69] Kay LE, Nicholson LK, Delaglio F, Bax A, Torchia DA. Pulse sequences for removal of the effects of cross correlation between dipolar and chemical-shift anisotropy relaxation mechanisms on the measurement of heteronuclear T1 and T2 values in proteins. J Magn Reson 1992;97:359–75.
[70] Mandel AM, Akke M, Palmer AG. Backbone dynamics of *Escherichia coli* ribonuclease HI: correlations with structure and function in an active enzyme. J Mol Biol 1995;246:144–63.
[71] Cole R, Loria JP. FAST-Modelfree: a program for rapid automated analysis of solution NMR spin-relaxation data. J Biomol NMR 2003;26:203–13.
[72] Delaglio F, Grzesiek S, Vuister GW, Zhu G, Pfeifer J, Bax A. NMRPipe: a multidimensional spectral processing system based on UNIX pipes. J Biomol NMR 1995;6:277–93.
[73] Vranken WF, Boucher W, Stevens TJ, Fogh RH, Pajon A, Llinas M, et al. The CCPN data model for NMR spectroscopy: development of a software pipeline. Proteins 2005;59:687–96.
[74] Rieping W, Habeck M, Bardiaux B, Bernard A, Malliavin TE, Nilges M. ARIA2: automated NOE assignment and data integration in NMR structure calculation. Bioinformatics 2007;23:381–2.
[75] Ulrich EL, Akutsu H, Doreleijers JF, Harano Y, Ioannidis YE, Lin J, et al. BioMagResBank. Nucleic Acids Res 2008;36:D402–8.